

UCLA

UCLA Previously Published Works

Title

FAP20 is required for flagellum assembly in *Trypanosoma brucei*.

Permalink

<https://escholarship.org/uc/item/2x037902>

Journal

Cell regulation, 35(11)

Authors

Shimogawa, Michelle

Jonnalagadda, Keya

Hill, Kent

Publication Date

2024-11-01

DOI

10.1091/mbc.E23-12-0497

Peer reviewed

FAP20 is required for flagellum assembly in *Trypanosoma brucei*

Michelle M. Shimogawa^{1,2,3}, Keya Jonnalagadda¹, and Kent L. Hill^{1,2,3,*}

¹Department of Microbiology, Immunology and Molecular Genetics, University of California Los Angeles, Los Angeles, CA 90095; ²California NanoSystems Institute, University of California Los Angeles, Los Angeles, CA 90095; ³Molecular Biology Institute, University of California Los Angeles, Los Angeles, CA 90095

ABSTRACT *Trypanosoma brucei* is a human and animal pathogen that depends on flagellar motility for transmission and infection. The trypanosome flagellum is built around a canonical "9+2" axoneme, containing nine doublet microtubules (DMTs) surrounding two singlet microtubules. Each DMT contains a 13-protofilament A-tubule and a 10-protofilament B-tubule, connected to the A-tubule by a conserved, non-tubulin inner junction (IJ) filament made up of alternating PACRG and FAP20 subunits. Here we investigate FAP20 in procyclic form *T. brucei*. A FAP20-NeonGreen fusion protein localized to the axoneme as expected. Surprisingly, FAP20 knockdown led to a catastrophic failure in flagellum assembly and concomitant lethality. This differs from other organisms, where FAP20 is required for normal flagellum motility, but generally dispensable for flagellum assembly and viability. Transmission electron microscopy demonstrates failed flagellum assembly in FAP20 mutants is associated with a range of DMT defects and defective assembly of the paraflagellar rod, a lineage-specific flagellum filament that attaches to DMT 4-7 in trypanosomes. Our studies reveal a lineage-specific requirement for FAP20 in trypanosomes, offering insight into adaptations for flagellum stability and motility in these parasites and highlighting pathogen versus host differences that might be considered for therapeutic intervention in trypanosome diseases.


SIGNIFICANCE STATEMENT


- Axoneme architecture and dynein-driven motility are conserved across eukaryotes, but mechanisms conferring lineage-specific motility are largely unknown. FAP20 is a flagellar protein that impacts motility in multiple organisms, but has not been studied in trypanosomes.
- This work demonstrates FAP20 is uniquely required for flagellum assembly and cell viability in *Trypanosoma brucei*, an early branching eukaryotic pathogen. Without FAP20, the axoneme, paraflagellar rod, and flagellum attachment zone are disrupted, causing lethal defects in cell division and morphogenesis.
- This work provides insight into pathogen adaptations for moving through host environments and illuminates targets to consider for therapeutic intervention in trypanosome diseases.

Monitoring Editor

Ke Hu
Arizona State University

Received: Jan 18, 2024
Revised: Sep 23, 2024
Accepted: Sep 25, 2024

 Challenge

 New Hypothesis

This article was published online ahead of print in MBoC in Press (<http://www.molbiolcell.org/cgi/doi/10.1091/mbc.E23-12-0497>) on October 25, 2024.

Author Contributions: M.M.S., K.J., and K.L.H. conceived and designed the experiments; M.M.S. and K.J. performed the experiments; M.M.S., K.J., and K.L.H.

INTRODUCTION

Trypanosoma brucei and related African trypanosomes are deadly pathogens of humans and other mammals that impose a tremendous burden on human health and prosperity throughout sub-Saharan Africa (Kristjanson et al., 1999; Abro et al., 2021). While dedicated efforts and development of new therapeutic options (Alvarez-Rodriguez et al., 2022; Valverde Mordt et al., 2022) have reduced the human health burden, these parasites remain a threat to the lives of 70 million people living in 36 countries (Papagni et al., 2023). Related kinetoplastid parasites, *Trypanosoma cruzi* and *Leishmania* spp., afflict almost a billion people worldwide (Rao et al., 2019). Meanwhile, *T. brucei* infection of agriculturally important livestock presents a substantial economic burden, with an estimated annual unrealized income of almost 5 billion dollars in endemic areas (Abro et al., 2021). Animals also serve as reservoirs of infection that limit efforts to eradicate the disease (Kasozi et al., 2023). Beyond their direct medical and economic importance, trypanosomatid parasites are valuable models for understanding fundamental eukaryote cell biology (Serricchio and Bütikofer, 2011; Vincensini et al., 2011; Lukeš et al., 2023). As such, there is great interest in understanding trypanosome biology.

T. brucei is a flagellated protozoan that is transmitted between mammalian hosts by a tsetse fly vector. Flagellum-mediated motility is required for transmission through the tsetse and for infection of a mammalian host (Rotureau et al., 2014; Shimogawa et al., 2018). *T. brucei* is an exclusively extracellular parasite and flagellated at all developmental stages throughout its life cycle. Its flagellum must be stable enough to support vigorous movement while laterally attached to the cell body, and withstand external forces encountered while moving through blood and tissues of the mammalian host and insect vector (Langousis and Hill, 2014; Imhof et al., 2019; Zhang et al., 2021). Beyond its role in motility, the *T. brucei* flagellum also directs cell morphogenesis (Kohl et al., 2003) and provides a platform for assembling signaling machinery that mediates host–pathogen interactions necessary for transmission and pathogenesis (Oberholzer et al., 2011; Salmon et al., 2012; Shaw et al., 2019; Velez-Ramirez et al., 2021; Bachmaier et al., 2023). Therefore, understanding flagellum structure and composition in trypanosomes has become a topic of great interest (Sáez Conde and Dean, 2022).

The trypanosome flagellum is composed of a canonical “9+2” axoneme, together with a lineage-specific paraflagellar rod (PFR) filament that is laterally connected to the axoneme along most of its length (Langousis and Hill, 2014). The 9+2 axoneme consists of nine outer doublet microtubules (DMTs) arranged around two singlet microtubules (Figure 1A). Each microtubule is made from α/β -tubulin dimers that polymerize end-to-end to form

protofilaments, which in turn connect laterally to form a cylinder (Downing and Nogales, 1998). DMTs contain one complete, 13-protofilament A-microtubule (A-tubule), connected to an incomplete, 10-protofilament B-microtubule (B-tubule) ([Nicastro et al., 2011], Figure 1A). Recent work in trypanosomes and other organisms has provided insight into proteins that mediate DMT assembly and function (Stoddard et al., 2018; Ichikawa et al., 2019; Imhof et al., 2019; Ma et al., 2019; Owa et al., 2019; Gui et al., 2021; Gui et al., 2022; Li et al., 2022; Kubo et al., 2023; Shimogawa et al., 2023). Of particular interest is the inner junction (IJ) that connects the B-tubule to the A-tubule at the inner face of each DMT (Yanagisawa et al., 2014; Dymek et al., 2019; Khalifa et al., 2020; Shimogawa et al., 2023). The IJ contains a non-tubulin filament together with microtubule inner proteins (MIPs) that interconnect with the IJ filament and each other, facilitating attachment of protofilament 10 of the B-tubule to protofilament 1 of the A-tubule (Yanagisawa et al., 2014; Dymek et al., 2019; Khalifa et al., 2020; Shimogawa et al., 2023) (Figure 1A). Unlike protofilaments, the IJ filament is a non-tubulin polymer of alternating PACRG and FAP20 subunits (Yanagisawa et al., 2014; Dymek et al., 2019). Most organisms contain a single PACRG, while some, such as trypanosomes and *Tetrahymena* (Kubo et al., 2023), contain two PACRG genes (Dawe et al., 2005; Kubo et al., 2023).

Studies in several organisms indicate PACRG and FAP20 are required for IJ filament assembly and axoneme motility, but generally dispensable for overall flagellum assembly (Laligne et al., 2010; Mendes Maia et al., 2014; Yanagisawa et al., 2014; Dymek et al., 2019; Chrystal et al., 2022; Gonzalez-Del Pozo et al., 2022; Chen et al., 2023). In *Chlamydomonas* for example, the DMT can even assemble with overall normal architecture in the complete absence of the IJ filament (Dymek et al., 2019). It is likely therefore, that MIP proteins around the IJ cooperate with the IJ filament to maintain B-tubule architecture and attachment to the A-tubule. In *T. brucei*, knockdown (KD) of either of the two PACRG homologues, PACRG-A or -B, did not affect cell growth or DMT assembly, while KD of both together slowed cell growth and led to DMT assembly defects that became progressively worse toward the distal end of the axoneme, although cells remained viable and overall flagellum length was not affected (Dawe et al., 2005). FAP20, the remaining IJ filament subunit, has not previously been studied in *T. brucei* and is the focus of the current work.

Here, we investigate *T. brucei* FAP20 function using a combination of inducible RNAi KD, fluorescence microscopy and thin-section transmission electron microscopy (TEM). Our results show that FAP20 is essential for flagellum assembly and cell viability, suggesting the unique importance of FAP20 and the IJ filament for flagellum stability and motility in this parasite.

RESULTS AND DISCUSSION

FAP20 KD is lethal in *T. brucei*

To study FAP20 function, we used tetracycline (Tet)-inducible RNAi KD against a portion of the *FAP20* open reading frame to generate a “FAP20 KD” cell line. RNAi was performed in procyclic cultured form (PCF) cells expressing an mNeonGreen (NG)-tagged version of FAP20 (FAP20-NG) and KD was confirmed by Western blot (Figure 1B). FAP20 protein was reduced within 24 h post-induction (hpi) and not detected by Western at 48hpi (Figure 1B). To our surprise, FAP20 KD was rapidly lethal, with cell doubling ceasing between 24 and 48hpi (Figure 1C; Supplemental Movie S1). An independent cell line, targeting the *FAP20* 3' untranslated region (UTR) (“FAP20 UTR KD”), exhibited the same

analyzed the data; M.M.S., K.J., and K.L.H. drafted the article; M.M.S. prepared the digital images.

Conflicts of interest: The authors declare no financial conflict of interest.

*Address correspondence to: Kent L. Hill (kenthill@microbio.ucla.edu).

Abbreviations used: CPC, central pair complex; CryoEM, cryogenic electron microscopy; DMT, doublet microtubule; FAZ, flagellum attachment zone; Hpi, hours post-induction; IJ, inner junction; KD, knockdown; MIP, microtubule inner protein; NG, mNeonGreen; PCF, procyclic cultured form; PFR, paraflagellar rod; RNAi, RNA interference; TEM, transmission electron microscopy; Tet, tetracycline; UTR, untranslated region.

© 2024 Shimogawa et al. This article is distributed by The American Society for Cell Biology under license from the author(s). Two months after publication it is available to the public under an Attribution–Noncommercial–Share Alike 4.0 Unported Creative Commons License (<http://creativecommons.org/licenses/by-nc-sa/4.0>).

“ASCB®,” “The American Society for Cell Biology®,” and “Molecular Biology of the Cell®” are registered trademarks of The American Society for Cell Biology.

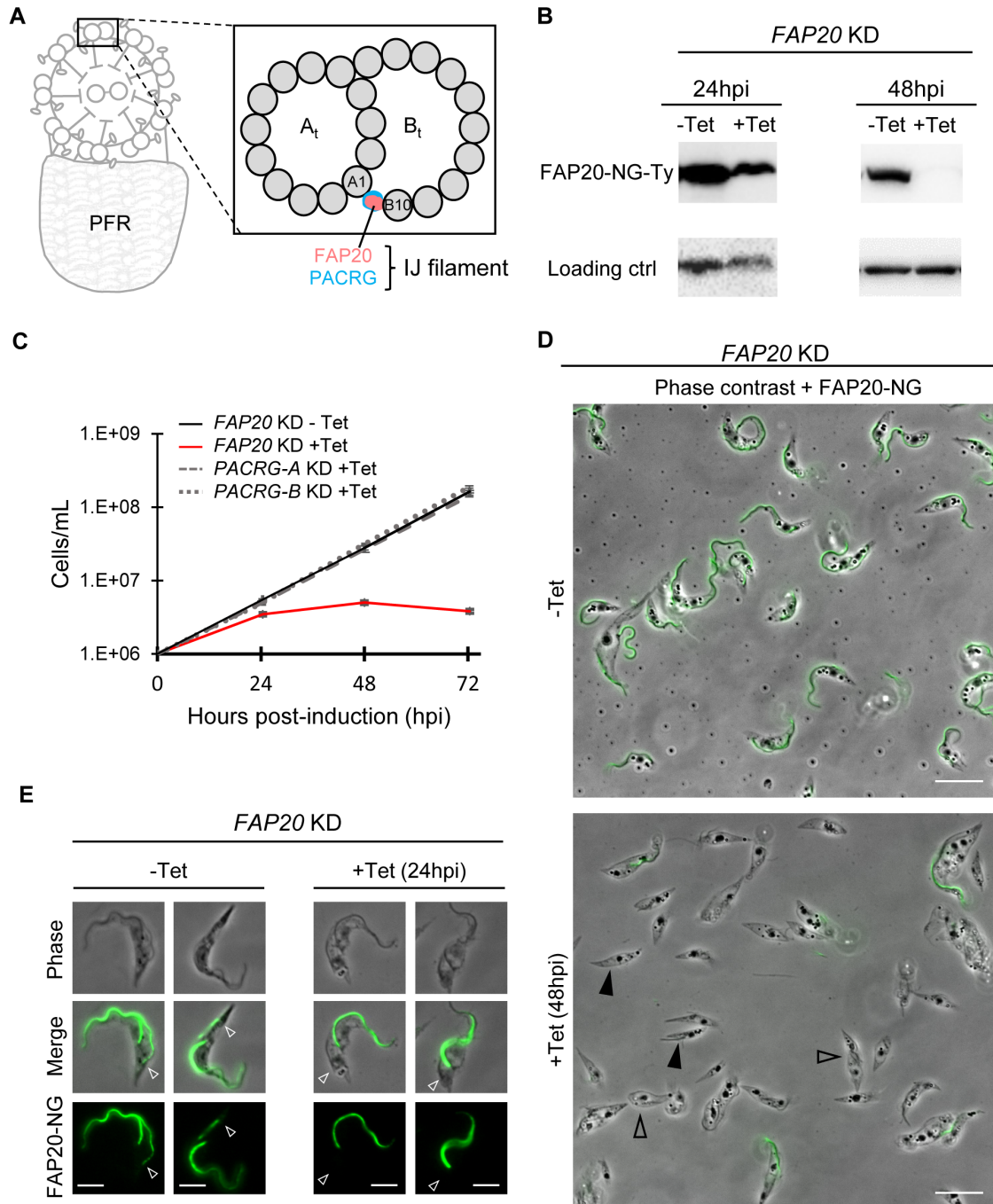


FIGURE 1: *FAP20* KD is lethal in *T. brucei*. (A) Cartoon showing a cross-section of the *T. brucei* flagellum comprised of a 9+2 axoneme and PFR. Inset shows a cross-section of a DMT with the A- and B-microtubules (A_t , B_t) labeled and tubulin protofilaments in gray. The IJ filament formed by *FAP20* and *PACRG* connects tubulin protofilaments A1 and B10. (B) *FAP20* KD parasites were grown in the presence of Tet to induce KD. Western blot analysis of *FAP20* protein expression, as detected with anti-Ty antibody, and anti-tubulin (24hpi) or anti-PFR2 (48hpi) as loading controls. A total of 5×10^6 cell equivalents were loaded per lane for anti-Ty (24hpi and 48hpi) and the 48hpi loading control (PFR2). A total of 2.5×10^6 cell equivalents per lane were loaded for the 24hpi loading control (tubulin). (C) Cumulative growth curve shows the mean cell density \pm SD versus time from two independent biological replicates (*FAP20* KD) or three independent biological replicates (*PACRG-A* KD and *PACRG-B* KD). (D) *FAP20* was knocked down by Tet-inducible RNAi in cells expressing *FAP20-NG* (green) and detergent-extracted cytoskeletons were prepared 48hpi. Open arrowheads show cells that are enlarged or failed in cell division. Black arrowheads show cells with short or absent flagella. Scale bar = 20 μ m. (E) Microscopy of fixed *FAP20* KD cells grown with or without Tet, showing dividing cells with two flagella. In *FAP20* KD cells +Tet (24hpi), *FAP20-NG* is retained in the old flagellum, but not assembled into the new flagellum (open arrowheads). Scale bar = 5 μ m.

lethal phenotype (Supplemental Movie S2). This result contrasts with what is observed following KD of either of the other two IJ subunits, PACRG-A or -B, which had no effect on cell growth (Figure 1C; Supplemental Figure S1), as reported previously (Dawe et al., 2005). Prior studies showed that simultaneous KD of both PACRG-A and -B did slow cell growth, although the defect was not evident until approximately 72hpi and cells remained viable (Dawe et al., 2005). The rapid, lethal phenotype of *FAP20* KD also differs from KD of *T. brucei* MIPs examined to date, which have minimal impact on parasite growth or viability (Shimogawa et al., 2023).

To better understand the nature of the lethal phenotype, we examined *FAP20* KD and *FAP20* UTR KD cells directly. Microscopic examination of fixed cells at 24hpi revealed that *FAP20* KD resulted in clumps of two or more cells that failed to separate, in some cases with abnormal morphologies (Supplemental Figure S2). Cell motility was severely compromised upon KD (Supplemental Movies S1 and S2). Control cells had vigorously beating flagella and generally moved propulsively with the flagellum tip leading, but *FAP20* KD and *FAP20* UTR KD cells were essentially immotile (Supplemental Movies S1 and S2). One cell in a clump occasionally retained an actively beating flagellum, but the others generally showed no indication of flagellar motility at all (Supplemental Movies 1 and 2). This is one of the most severe motility defects described for KD of flagellar proteins in *T. brucei*. Many mutants lack normal cell propulsion, but retain a beating flagellum, and typically fail at the final stage of cell septation, yielding clusters of multiple cells having mostly normal morphology, but connected at their posterior ends (Bastin et al., 1998; Branche et al., 2006; Baron et al., 2007; Rotureau et al., 2014). In contrast, the cell division phenotype in *FAP20* KD cells is reminiscent of mutants that disrupt intraflagellar transport and flagellum attachment zone (FAZ) assembly, which exhibit severe defects in flagellum assembly, disrupted cell division and abnormal cell morphologies (Kohl et al., 2003; Absalon et al., 2008; Zhou et al., 2011; Sunter et al., 2015; An et al., 2020). The combined defects—lethality, catastrophic cell division defects, and severe disruption of flagellar motility—demonstrate a critical requirement for *FAP20* in flagellum assembly and function in this organism.

FAP20* KD blocks flagellum and FAZ assembly in *T. brucei

T. brucei's prominent flagellum is clearly visible as a dark line in phase contrast images (Figure 1, D and E) and *FAP20*-NG is localized along the flagellum (Figure 1, D and E; Billington et al., 2023), as expected. *FAP20*-NG is completely lost in most cells of the *FAP20* KD, although a small number of cells retain *FAP20*-NG at near-uninduced levels, even at 48hpi (Figure 1D). Replication of the trypanosome flagellum is a conservative process, with one daughter cell inheriting the "old" flagellum that was assembled during a previous cell cycle, and the other daughter cell inheriting a "new" flagellum assembled in the current cell cycle (Sherwin and Gull, 1989). Examination of dividing cells with two flagella confirms that *FAP20* depletion specifically affects the new flagellum (Figure 1E), which is readily identified as always located posterior to the old flagellum (Sherwin and Gull, 1989). Thus, the cells that retain *FAP20*-NG after Tet induction likely represent flagella that assembled prior to *FAP20* depletion. These results are consistent with published data showing that *FAP20* in *Chlamydomonas* does not readily turn over once incorporated into the flagellum (Yanagisawa et al., 2014).

In cells lacking *FAP20*-NG, the flagellum appears short or absent (Figure 1D), indicating loss of *FAP20* disrupts assembly of the entire flagellum. We therefore used immunofluorescence against

the PFR as a flagellum marker (Saada et al., 2014). Samples were examined at 24hpi because that is the first timepoint assessed where the growth defect was evident. In control cells, *FAP20*-NG signal localized alongside the PFR, from the distal tip of the flagellum past the proximal end of the PFR (Figure 2A), as expected for an axonemal protein (Kohl et al., 1999). In *FAP20* KD cultures, cells without *FAP20*-NG have a short and sometimes misshapen PFR (Figure 2, A and B), demonstrating that flagellum assembly is ultimately blocked. In cells that retained *FAP20*-NG, the *FAP20*-NG signal stopped substantially before the end of the PFR at the distal tip of the flagellum (Figure 2A, arrowheads), presumably corresponding to cells in which PFR assembly continued after *FAP20* KD. Assembly of the PFR depends on flagellum assembly (Kohl et al., 2003); therefore, the defects in PFR assembly are likely due to the inability of cells to form a stable flagellum in the absence of *FAP20*.

To further examine the impact of *FAP20* KD, we conducted cell cycle analysis using PFR immunofluorescence and DNA staining of the kinetoplast (K) and nucleus (N) as markers (Figure 3). *FAP20* KD cells (17hpi) were predominantly 1K1N, frequently with short or missing flagella (Figure 3, A and B), and the proportion of cells with two flagella decreased from 31% (39 of 126 cells) in uninduced cultures to 18% (29 of 157 cells) after 17 h of KD. In cases where cells had started to assemble a new flagellum, *FAP20* KD cells mostly exhibited 1K1N or 1K2N configurations, instead of the typical 2K1N or 2K2N configurations seen in uninduced cells (Figure 3, A and B), consistent with kinetoplast duplication and separation defects associated with defective flagellum assembly (Kohl et al., 2003; Absalon et al., 2008). Thus, cell cycle analysis supports the idea that cells lacking *FAP20* are unable to form new flagella. The observed block in flagellum assembly (Figures 2 and 3), distinguishes the *FAP20* KD from other axoneme protein KDs, which generally assemble normal length flagella (Dawe et al., 2005; Baron et al., 2007; Shimogawa et al., 2023; Supplemental Figure S1). Moreover, the data distinguish the PCF *FAP20* KD phenotype from that of bloodstream form flagellar mutants, which fail at cleavage furrow ingression but continue through multiple rounds of axoneme and PFR replication (Ralston and Hill, 2006).

The *FAP20* KD cell division defects are reminiscent of those seen upon disruption of the FAZ, which directs positioning of cytokinetic machinery (Kohl et al., 2003; Absalon et al., 2008; Sunter et al., 2015; An et al., 2020). Blocking flagellum assembly disrupts FAZ assembly (Kohl et al., 2003), suggesting the *FAP20* KD cell division defect may be a consequence of disrupting the FAZ. To test this idea, we used antibodies against FAZ1 (Kohl et al., 1999) to ask whether loss of *FAP20* disrupts FAZ assembly. Cells lacking *FAP20*-NG frequently displayed short or aberrant FAZ structures (Figure 2C). The combined data demonstrate that *FAP20* is critical for stable assembly of the flagellum and FAZ, which, in turn, are required for progression of cell division.

***FAP20* is required for stable flagellum assembly uniquely in *T. brucei*, indicating a critical role for the IJ in this pathogen**

To elucidate ultrastructural foundations of the *FAP20* KD flagellum assembly defect, we examined cells by thin-section TEM. At low magnification, the flagellum defect is clearly evident, as fewer flagella were observed in *FAP20* KD versus control sections (Figure 4A). When examined at higher resolution, control cells were seen to contain a canonical 9+2 arrangement of axonemal microtubules (Figure 4B). *FAP20* KD cells, on the other hand, exhibited a range of DMT defects, including singlets, incomplete doublets, displaced doublets, and extranumerary doublets (Figure 4B). Axonemal

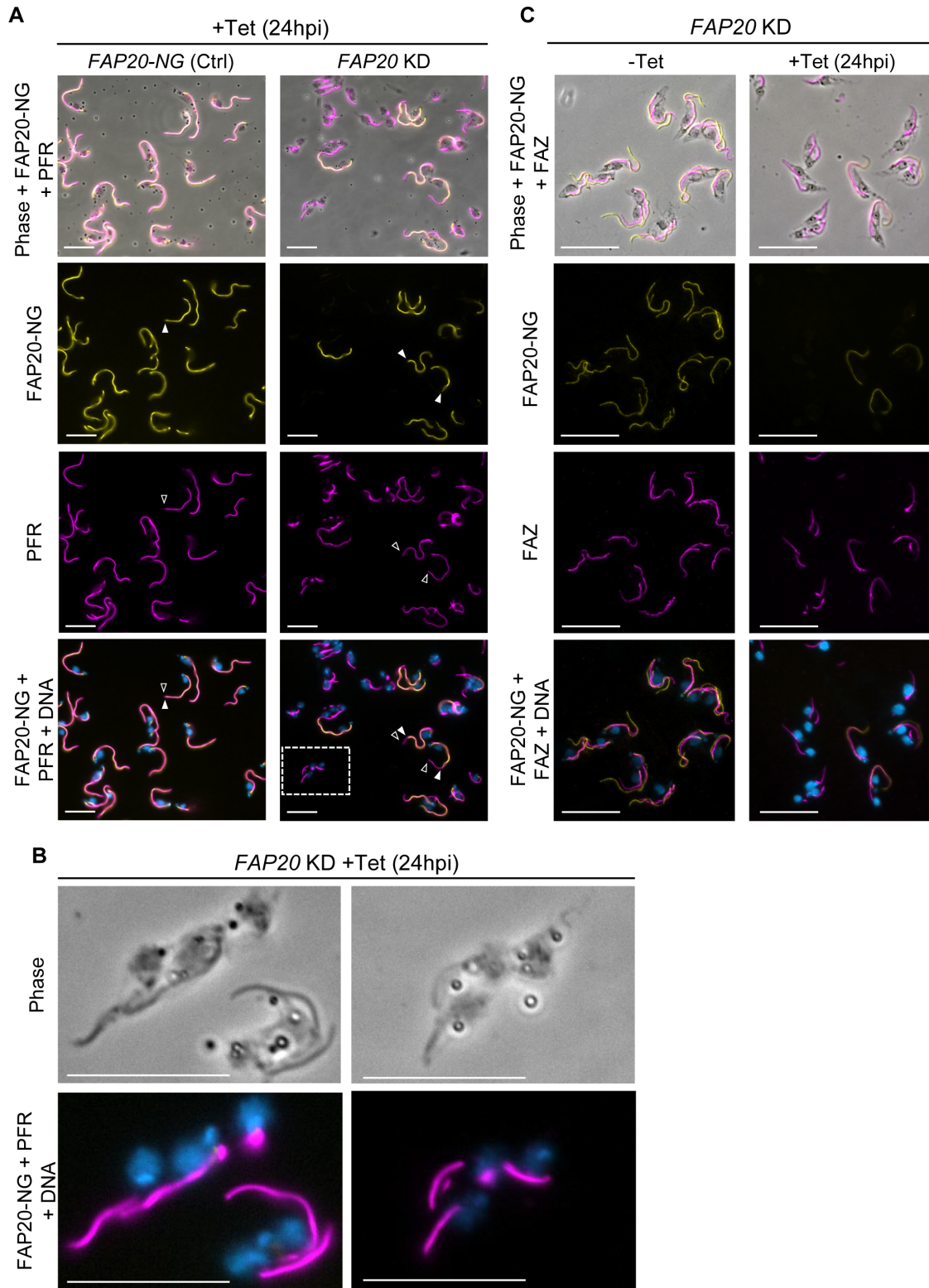


FIGURE 2: FAP20 KD disrupts flagellum and FAZ assembly. (A) Detergent-extracted cytoskeletons were prepared from FAP20-NG (Ctrl) and FAP20 KD parasites grown in Tet for 24 h to induce KD. Images show NG-tagged FAP20 (yellow), PFR (magenta) and DNA (blue). Scale bar = 20 μ m. Images are representative of at least two independent experiments. The distal end of FAP20 signal is indicated by a closed arrowhead, while the distal end of PFR signal is indicated with an open arrowhead. The area boxed by a white dashed line is enlarged in panel B (right). (B) Enlarged images of FAP20 KD cells lacking detectable FAP20-NG and with aberrant PFR. (C) Detergent-extracted cytoskeletons were prepared from FAP20 KD parasites grown in the absence or presence of Tet for 24 h to induce KD. Images show FAP20-NG (yellow), the FAZ (magenta) and DNA (blue). Scale bar = 20 μ m.

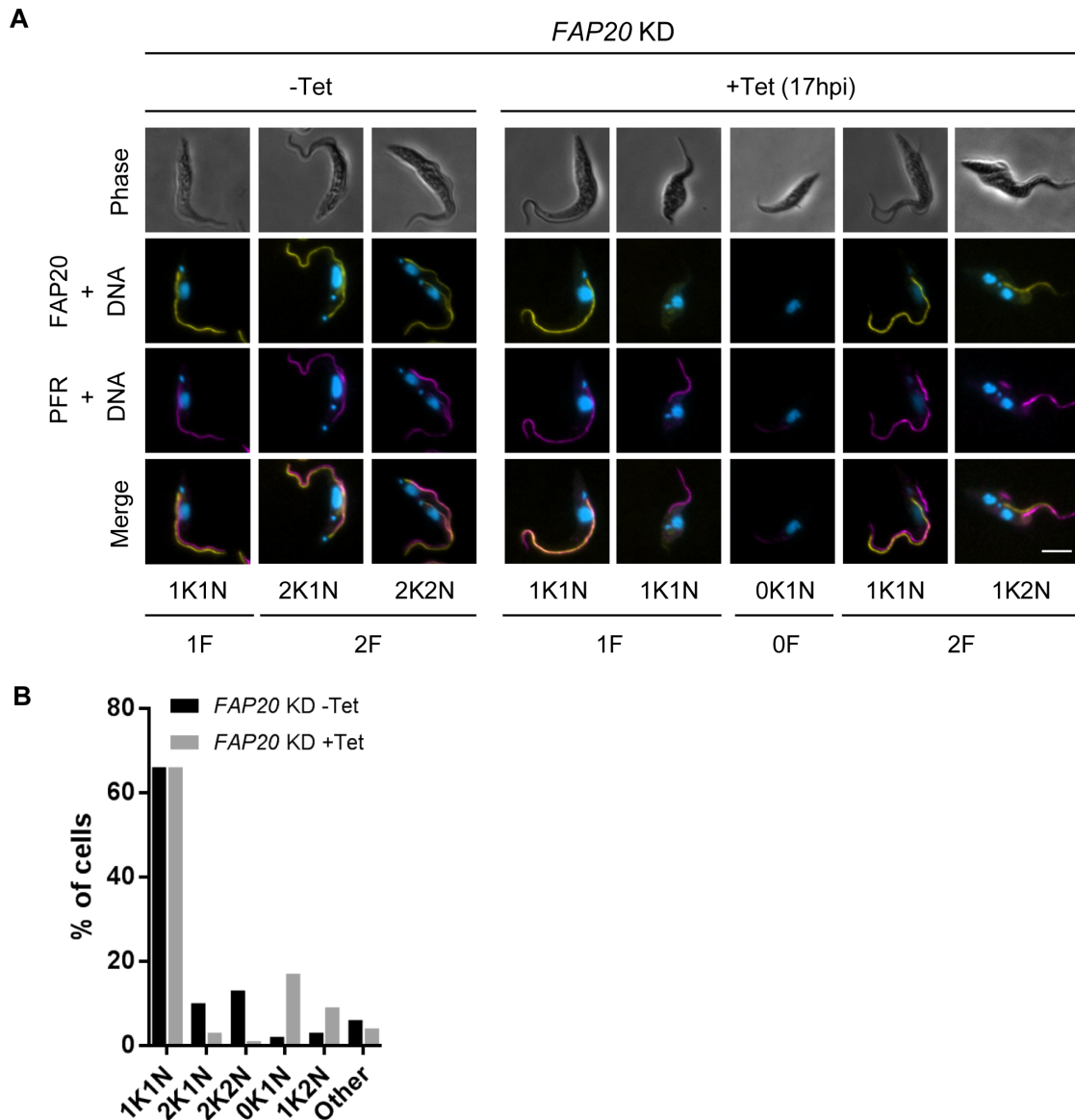


FIGURE 3: Cell cycle analysis of *FAP20* KD. (A) Fluorescence microscopy of fixed cells showing examples of observed cell cycle stages 17 h after induction of *FAP20* KD. Antibody against PFR (magenta) was used to mark the flagellum (F). Kinetoplast (K) and nuclear (N) DNA were stained with Hoechst (blue). Uninduced cells (–Tet) show FAP20-NG (yellow) in all flagella, while flagella in induced cells (+Tet) were either FAP20-NG positive or negative, presumably depending on whether the flagellum assembled prior to depletion of *FAP20*. (B) Images from the experiment shown in panel A were used to score cells according to their cell cycle stage. –Tet N = 126, +Tet N = 157.

defects were primarily restricted to DMTs and obvious defects in the central pair were rarely observed, except in sections where the entire axoneme was distorted. Occasionally we observed PFR defects, for example, incomplete or excessive PFR material (Figure 4B), consistent with PFR immunofluorescence results (Figure 2, A and B). Prior work has shown PFR assembly depends on axoneme assembly, though details are not clear (Kohl et al., 2003), and we therefore suspect PFR defects are an indirect consequence of defective axoneme assembly in *FAP20* KD cells.

Our combined data demonstrate that loss of *FAP20* is lethal in *T. brucei* due to severe defects in assembly of DMTs and ultimate failure of flagellum assembly. Cryogenic electron microscopy (CryoEM) analysis indicates *FAP20* of *Chlamydomonas* is found at

both the IJ of the DMT and at the base of the C2a projection of the central pair complex (CPC) (Yanagisawa et al., 2014; Dymek et al., 2019; Gui et al., 2022). While we cannot formally distinguish between a CPC defect versus an IJ defect as the source of the *FAP20* KD phenotype, TEM data demonstrate prominent DMT defects and little to no detectable disruption of the CPC (Figure 4B). Moreover, KD of CPC proteins in *T. brucei* does not block flagellum assembly and is not lethal (Branche et al., 2006; Ralston et al., 2006). Therefore, we favor the idea that flagellum assembly failure and concomitant lethal phenotype are due to requirement of *FAP20* at the IJ.

FAP20 function has been studied in several organisms, where mutants show defective ciliary motility, perturbation of the IJ

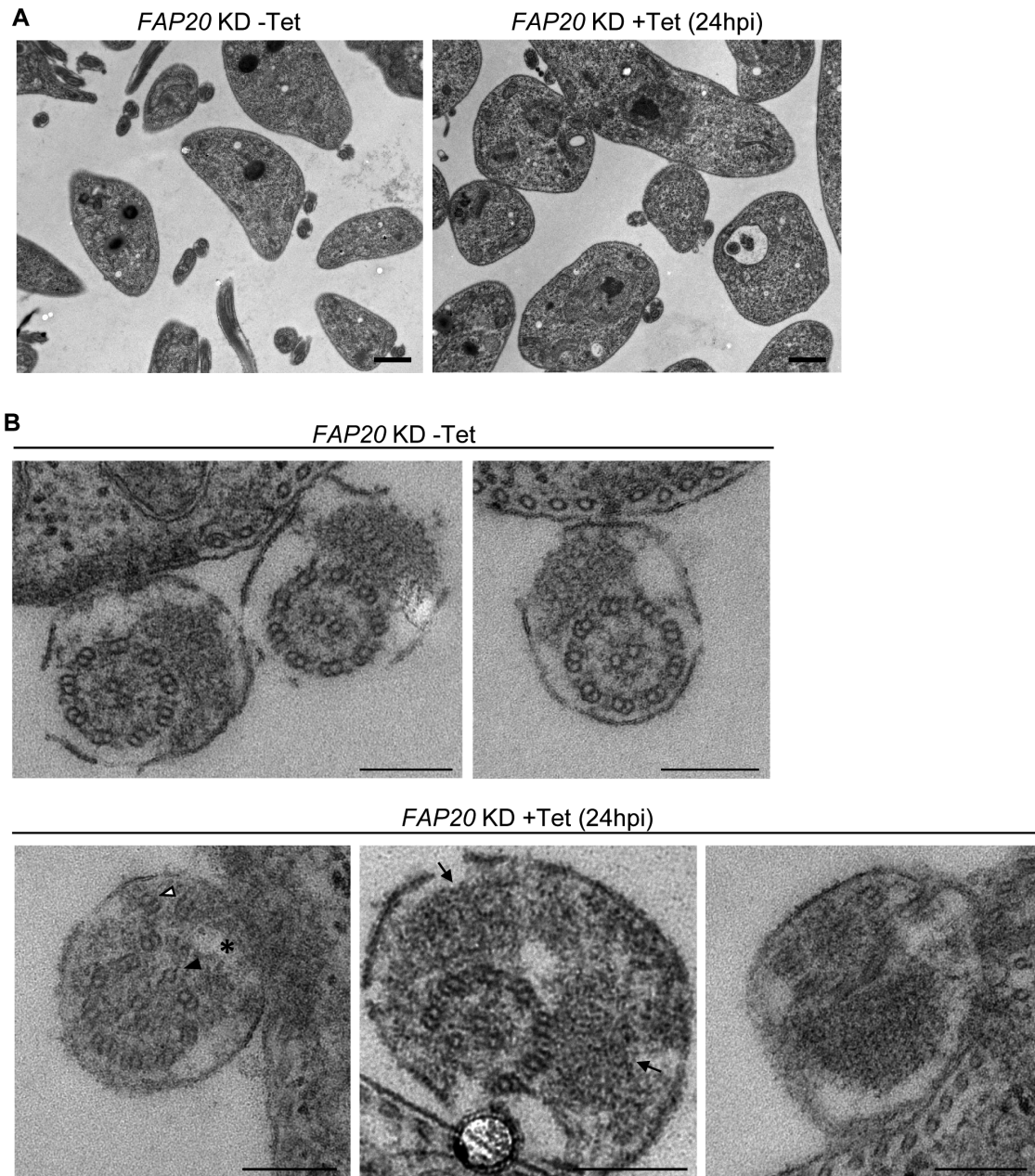


FIGURE 4: FAP20 KD disrupts flagellum ultrastructure. (A) Representative thin-section TEM images of FAP20 KD cells without tetracycline (–Tet) and after 24 h Tet-induction. Scale bar = 1 μ m. Images are representative of two independent experiments. (B) TEM images of individual flagella, showing examples of displaced, extranumerary doublets (open arrowhead), singlets or incomplete doublets (arrowheads), incomplete PFR (*) or excessive PFR (arrows). Scale bar = 200 nm. Images are representative of two independent experiments.

filament, and reduced axoneme stability, albeit without blocking assembly of the flagellum, which grows to mostly normal length and in some cases longer (Laligne *et al.*, 2010; Mendes Maia *et al.*, 2014; Yanagisawa *et al.*, 2014; Dymek *et al.*, 2019; Chrystal *et al.*, 2022; Gonzalez-Del Pozo *et al.*, 2022; Chen *et al.*, 2023). Recent studies have shown that FAP20 can directly connect tubulin dimers to intact microtubules *in vitro*, and enhance microtubule stability (Banger *et al.*, 2023). These *in vitro* studies provide a biochemical basis for FAP20 in connecting tubulin protofilaments of the A- and B-tubules at the IJ and promoting axoneme stability. Notably, however, in no case did loss of FAP20 block flagellum assembly

in other organisms. In many instances, the DMT exhibited mostly normal architecture despite absence of FAP20 and, in some cases, even complete absence of the entire IJ filament (Dymek *et al.*, 2019). Thus, in other organisms, FAP20 contributes to but is not required for DMT assembly and stability, whereas loss of FAP20 in *T. brucei* leads to rapid and complete failure of stable flagellum assembly and is lethal. Indeed, this is one of the most severe defects reported for a flagellar protein in PCF *T. brucei* cells (Kohl *et al.*, 2003; Dawe *et al.*, 2005; Branche *et al.*, 2006; Baron *et al.*, 2007; Absalon *et al.*, 2008; Ralston and Hill, 2008). A potential explanation for lineage-specific dependency on FAP20 in *T. brucei*

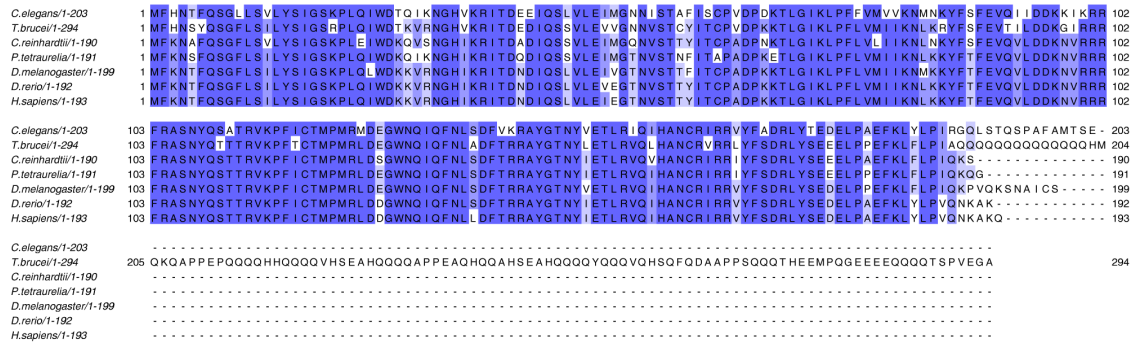


FIGURE 5: Clustal Omega alignment of FAP20 protein sequences from organisms in which FAP20 function has been studied. *T. brucei* FAP20 has a long C-terminal poly-glutamine (poly-Q)-rich domain that is not present in organisms that do not require FAP20 for flagellum assembly.

is the lineage-specific poly-glutamine (poly-Q)-rich C-terminal extension that is uniquely found on the *T. brucei* protein compared to FAP20 from all other organisms in which FAP20 function has been studied (Figure 5). Given the extensive interconnections among IJ subunits and MIPs of the DMT (Khalifa et al., 2020; Shimogawa et al., 2023), together with numerous lineage-specific trypanosome MIPs (Imhof et al., 2019; Shimogawa et al., 2023), it is conceivable that loss of FAP20 disrupts a trypanosome-specific interaction with other trypanosome proteins critical for flagellum assembly. As has been noted previously (Heddergott et al., 2012; Bargul et al., 2016; Imhof et al., 2019), several constraints (e.g., attachment to the PFR and cell body, vigorous, three-dimensional beating, and encounters with host tissues) impose unique demands on axoneme stability in trypanosomes (Imhof et al., 2019). These constraints might make the need for FAP20 in supporting axoneme stability particularly acute in trypanosomes.

While the underlying basis for FAP20 dependency in trypanosomes remains to be determined, our combined results underscore the importance of FAP20, and the IJ filament, for flagellum stability and motility in trypanosomes relative to other flagellated eukaryotic cells, and suggest FAP20 may accommodate unique adaptations required for the parasite to move through its insect vector and vertebrate host. As trypanosomes are medically and economically important pathogens, our results highlight a difference between pathogen and host that might be exploited for therapeutic intervention.

MATERIALS AND METHODS

[Request a protocol through Bio-protocol](#)

Biological materials

All novel biological materials are available from the authors upon request.

***T. brucei* culture.** Procyclic *T. brucei brucei* (strain 29-13) originally obtained from George Cross (Rockefeller University) (Wirtz et al., 1999) were cultivated in SM medium (Oberholzer et al., 2009) supplemented with 10% heat-inactivated FBS at 28°C with 5% CO₂.

***In situ* tagging.** NG-tagged cell lines were generated in the 29-13 background by C-terminal tagging (Dean et al., 2015) with pPOTv6-puro-puro-NG. See Supplemental Table S1 for list of primers.

Tet-inducible KD. Constructs for Tet-inducible KD were designed using RNAit (Redmond et al., 2003) and cloned into p2T7-177 (Wickstead et al., 2002). See Supplemental Table S1 for list of primers. NotI-linearized plasmids were transfected into the corresponding NG-tagged cell lines using established methods (Oberholzer et al., 2009). Clonal lines were generated by limiting dilution. KD was induced by growing cells in the presence of 1 µg/ml Tet. For growth curves, cells were counted with a Beckman Coulter Z1 particle counter and diluted daily to a concentration of 1 × 10⁶ cells/ml.

Western blotting. Cells were washed in Dulbecco's phosphate buffered saline (DPBS) and boiled in 1x Laemmli sample buffer (Bio-Rad). Samples were separated on a 10% acrylamide gel and transferred to nitrocellulose membrane. Membranes were blocked in PBS + 5% milk and incubated overnight at 4°C in primary antibody diluted in blocking solution (1:3000 mouse anti-Ty BB2 (Bastin et al., 1996), 1:10,000 mouse anti-beta tubulin E7 (Developmental Studies Hybridoma Bank), or 1:10,000 rabbit anti-PFR2 [Saada et al., 2014]). Membranes were washed three times in PBS + 0.05% Tween-20 (PBS-T) and incubated in horseradish peroxidase-conjugated goat anti-mouse or goat anti-rabbit secondary antibody (Bio-Rad) diluted 1:5000 in blocking solution. After washing three times in PBS-T, membranes were developed using the SuperSignal West Pico PLUS chemiluminescent substrate kit (Thermo Fisher Scientific) and images were captured on a Bio-Rad Chemi-Doc MP imaging system.

Video microscopy. Cells were applied to a glass slide and covered with a glass coverslip. Videos were acquired at ~30 fps on a Zeiss Axiovert 200M microscope with a 40x objective lens using a Basler ace acA5472-17um camera and Pylon software. Videos were cropped in Fiji and played back at 30 fps.

Microscopy of fixed whole cells

Cells were washed in PEME buffer (100 mM PIPES, 2 mM EGTA, 1 mM MgSO₄, 0.1 mM EDTA, pH 6.8) and resuspended in DPBS. Cells were fixed with 0.2% paraformaldehyde on ice for 5 min, washed in DPBS and allowed to dry onto poly-L-lysine-treated coverslips. Coverslips were permeabilized in -20°C methanol for 30 s, dried, and rehydrated in DPBS (Supplemental Figure S2) or permeabilized in DPBS + 0.1% Triton X-100 for 10 min and rinsed in DPBS (Figure 1E) before mounting on slides. Images were acquired on a Zeiss Axioskop II microscope with a Plan-Apochromat 63x/1.4 objective lens using Zen software.

Fluorescence microscopy of detergent-extracted cytoskeletons

Cells were washed in PEME buffer, resuspended in DPBS and allowed to settle onto poly-L-lysine-treated coverslips for 10 min. Nonadhered cells were removed and cytoskeletons were extracted on the coverslip for 5 min in PEME + 1% IGEPAL CA-630 (NP-40). Coverslips were rinsed in PEME and mounted directly on microscope slides or processed for immunofluorescence to detect the PFR or FAZ, as follows. Coverslips were blocked in DPBS + 8% normal donkey serum + 2% BSA, then incubated with 1:1000 rabbit anti-PFR2 (Saada *et al.*, 2014) or 1:10 mouse anti-FAZ1 IgG L3B2 (Kohl *et al.*, 1999) primary antibody diluted in blocking solution. Coverslips were washed three times for 10 min in DPBS + 0.05% Tween-20 (DPBS-T) and incubated with 1:1500 donkey anti-rabbit or donkey anti-mouse Alexa 594 secondary antibody (Invitrogen) diluted in blocking solution. Coverslips were washed three times as above, stained with Hoechst 33342 (Thermo Fisher Scientific), rinsed in DPBS and mounted on slides. Images were acquired on a Zeiss Axioskop II microscope with a Plan-Apochromat 40x/1.4 or 63x/1.4 objective lens or a Zeiss Axio Imager Z1 fluorescence microscope with a Plan-Apochromat 63x/1.4 objective lens using Zen software.

Cell cycle analysis

Cells were washed in PEME buffer, resuspended in DPBS, and allowed to dry onto poly-L-lysine-treated coverslips. Coverslips were permeabilized in -20°C methanol for 30 s, dried, and rehydrated in DPBS, then processed as above to detect PFR and DNA. Cell cycle stage was scored according to the number of kinetoplasts and nuclei observed (Robinson *et al.*, 1995).

Thin-section TEM

Cells were fixed directly in cell culture medium by addition of 2.5% glutaraldehyde (Electron Microscopy Sciences) and pelleted. Cell pellets were resuspended in 4% paraformaldehyde + 2.5% glutaraldehyde in 0.1 M sodium cacodylate buffer, pH 7.2 (Electron Microscopy Sciences) and incubated for 1 h. Cells were pelleted and resuspended in fresh fixative solution and processed as follows at the Electron Core Facility, UCLA Brain Research Institute (all reagents and materials from Ted Pella). After wash, samples were embedded in 4% agarose gel and postfixed in 1% osmium tetroxide. After wash, samples were dehydrated through a graded series of ethanol concentrations and propylene oxide. After infiltration with Eponate 12 resin, the samples were embedded in fresh Eponate 12 resin and polymerized at 60°C for 48 h. Ultrathin sections of 70 nm thickness were prepared and placed on formvar carbon coated copper grids and stained with uranyl acetate and lead citrate. The grids were examined using a JEOL 100CX transmission electron microscope at 60 kV and images were captured by an AMT digital camera (Advanced Microscopy Techniques Corporation, model XR611). Two independent biological replicates were fixed and examined for each sample ($-/+$ Tet).

ACKNOWLEDGMENTS

Funding was provided by grant AI052348 (K.L.H.). K.J. was supported by the Beckman Scholars Program (Beckman Foundation). We thank Dr. Chunni Zhu at the UCLA Brain Research Institute Electron Microscopy Core Facility for TEM analysis and Angeline Wijono for technical assistance. We thank Elissa Hallem and Peter Bradley for use of their camera and microscope for collecting

videos and microscopy images. We also thank Jack Sunter for providing anti-FAZ antibodies.

REFERENCES

- Abro Z, Kassie M, Muriithi B, Okal M, Masiga D, Wanda G, Gisele O, Samuel A, Nguertoum E, Nina RA, *et al.* (2021). The potential economic benefits of controlling trypanosomiasis using waterbuck repellent blend in sub-Saharan Africa. *PLoS One* 16, e0254558.
- Absalon S, Blisnick T, Kohl L, Toutirais G, Dore G, Julkowska D, Tavenet A, Bastin P (2008). Intraflagellar transport and functional analysis of genes required for flagellum formation in trypanosomes. *Mol Biol Cell* 19, 929–944.
- Alvarez-Rodriguez A, Jin BK, Radwanska M, Magez S (2022). Recent progress in diagnosis and treatment of Human African Trypanosomiasis has made the elimination of this disease a realistic target by 2030. *Front Med (Lausanne)* 9, 1037094.
- An T, Zhou Q, Hu H, Cormaty H, Li Z (2020). FAZ27 cooperates with FLAM3 and ClpGM6 to maintain cell morphology in *Trypanosoma brucei*. *J Cell Sci* 133, jcs245258.
- Bachmaier S, Gould MK, Polatoglou E, Omelianczyk R, Brennan AE, Aloraini MA, Munday JC, Horn D, Boshart M, de Koning HP (2023). Novel kinetoplastid-specific cAMP binding proteins identified by RNAi screening for cAMP resistance in *Trypanosoma brucei*. *Front Cell Infect Microbiol* 13, 1204707.
- Bangera M, Dungdung A, Prabhu S, Sirajuddin M (2023). Doublet microtubule inner junction protein FAP20 recruits tubulin to the microtubule lattice. *Structure* 31, 1535–1544.e4.
- Bargul JL, Jung J, McOdimba FA, Omogo CO, Adung'a VO, Krüger T, Masiga DK, Engstler M (2016). Species-specific adaptations of trypanosome morphology and motility to the mammalian host. *PLoS Pathog* 12, e1005448.
- Baron DM, Kabututu ZP, Hill KL (2007). Stuck in reverse: loss of LC1 in *Trypanosoma brucei* disrupts outer dynein arms and leads to reverse flagellar beat and backward movement. *J Cell Sci* 120, 1513–1520.
- Baron DM, Ralston KS, Kabututu ZP, Hill KL (2007). Functional genomics in *Trypanosoma brucei* identifies evolutionarily conserved components of motile flagella. *J Cell Sci* 120, 478–491.
- Bastin P, Bagherzadeh Z, Matthews KR, Gull K (1996). A novel epitope tag system to study protein targeting and organelle biogenesis in *Trypanosoma brucei*. *Mol Biochem Parasitol* 77, 235–239.
- Bastin P, Sherwin T, Gull K (1998). Paraflagellar rod is vital for trypanosome motility. *Nature* 391, 548.
- Billington K, Halliday C, Madden R, Dyer P, Barker AR, Moreira-Leite FF, Carington M, Vaughan S, Hertz-Fowler C, Dean S, *et al.* (2023). Genome-wide subcellular protein map for the flagellate parasite *Trypanosoma brucei*. *Nat Microbiol* 8, 533–547.
- Branche C, Kohl L, Toutirais G, Buisson J, Cosson J, Bastin P (2006). Conserved and specific functions of axoneme components in trypanosome motility. *J Cell Sci* 119, 3443–3455.
- Chen Z, Li M, Zhu H, Ou G (2023). Modulation of inner junction proteins contributes to axoneme differentiation. *Proc Natl Acad Sci USA* 120, e2303955120.
- Crystal PW, Lambacher NJ, Doucette LP, Bellingham J, Schiff ER, Noel NCL, Li C, Tsiropoulou S, Casey GA, Zhai Y, *et al.* (2022). The inner junction protein CFAP20 functions in motile and non-motile cilia and is critical for vision. *Nat Commun* 13, 6595.
- Dawe HR, Farr H, Portman N, Shaw MK, Gull K (2005). The Parkin co-regulated gene product, PACRG, is an evolutionarily conserved axonemal protein that functions in outer-doublet microtubule morphogenesis. *J Cell Sci* 118, 5421–5430.
- Dean S, Sunter J, Wheeler RJ, Hodkinson I, Gluenz E, Gull K (2015). A toolkit enabling efficient, scalable and reproducible gene tagging in trypanosomatids. *Open Biol* 5, 140197.
- Downing KH, Nogales E (1998). Tubulin and microtubule structure. *Curr Opin Cell Biol* 10, 16–22.
- Dymek EE, Lin J, Fu G, Porter ME, Nicastro D, Smith EF (2019). PACRG and FAP20 form the inner junction of axonemal doublet microtubules and regulate ciliary motility. *Mol Biol Cell* 30, 1805–1816.
- Gonzalez-Del Pozo M, Fernandez-Suarez E, Bravo-Gil N, Mendez-Vidal C, Martin-Sanchez M, Rodriguez-de la Rúa E, Ramos-Jimenez M, Morillo-Sanchez MJ, Borrego S, Antinolo G (2022). A comprehensive WGS-based pipeline for the identification of new candidate genes in inherited retinal dystrophies. *NPJ Genom Med* 7, 17.

- Gui M, Croft JT, Zabeo D, Acharya V, Kollman JM, Burgoyne T, Hoog JL, Brown A (2022). SPACA9 is a luminal protein of human ciliary singlet and doublet microtubules. *Proc Natl Acad Sci USA* 119, e2207605119.
- Gui M, Farley H, Anujan P, Anderson JR, Maxwell DW, Whitchurch JB, Botsch JJ, Qiu T, Meleppattu S, Singh SK, et al. (2021). De novo identification of mammalian ciliary motility proteins using cryo-EM. *Cell* 184: 5791–5806.e19.
- Gui M, Wang X, Dutcher SK, Brown A, Zhang R (2022). Ciliary central apparatus structure reveals mechanisms of microtubule patterning. *Nat Struct Mol Biol* 29, 483–492.
- Heddergott N, Kruger T, Babu SB, Wei A, Stellamanns E, Uppaluri S, Pfohl T, Stark H, Engstler M (2012). Trypanosome motion represents an adaptation to the crowded environment of the vertebrate bloodstream. *PLoS Pathog* 8, e1003023.
- Ichikawa M, Khalifa AAZ, Kubo S, Dai D, Basu K, Maghrebi MAF, Vargas J, Bui KH (2019). Tubulin lattice in cilia is in a stressed form regulated by microtubule inner proteins. *Proc Natl Acad Sci USA* 116, 19930–19938.
- Imhof S, Zhang J, Wang H, Bui KH, Nguyen H, Atanasov I, Hui WH, Yang SK, Zhou ZH, Hill KL (2019). Cryo electron tomography with volta phase plate reveals novel structural foundations of the 96-nm axonemal repeat in the pathogen. *Elife* 8, e52058.
- Kasozi KI, MacLeod ET, Welburn SC (2023). African animal trypanocide resistance: A systematic review and meta-analysis. *Front Vet Sci* 9, 950248.
- Khalifa AAZ, Ichikawa M, Dai D, Kubo S, Black CS, Peri K, McAlear TS, Veyron S, Yang SK, Vargas J, et al. (2020). The inner junction complex of the cilia is an interaction hub that involves tubulin post-translational modifications. *Elife* 9, e527760.
- Kohl L, Robinson D, Bastin P (2003). Novel roles for the flagellum in cell morphogenesis and cytokinesis of trypanosomes. *EMBO J* 22, 5336–5346.
- Kohl L, Sherwin T, Gull K (1999). Assembly of the paraflagellar rod and the flagellum attachment zone complex during the trypanosoma brucei cell cycle. *J Eukaryot Microbiol* 46, 105–109.
- Kristjanson PM, Swallow BM, Rowlands GJ, Kruska RL, de Leeuw PN (1999). Measuring the costs of African animal trypanosomosis, the potential benefits of control and returns to research. *Agric Syst* 59, 79–98.
- Kubo S, Black CS, Joachimiak E, Yang SK, Legal T, Peri K, Khalifa AAZ, Ghanaeian A, McCafferty CL, Valente-Paterno M, et al. (2023). Native doublet microtubules from Tetrahymena thermophila reveal the importance of outer junction proteins. *Nat Commun* 14, 2168.
- Laligne C, Klotz C, de Loubresse NG, Lemullois M, Hori M, Laurent FX, Papon JF, Louis B, Cohen J, Koll F (2010). Bug22p, a conserved centrosomal/ciliary protein also present in higher plants, is required for an effective ciliary stroke in Paramecium. *Eukaryot Cell* 9, 645–655.
- Langousis G, Hill KL (2014). Motility and more: the flagellum of Trypanosoma brucei. *Nat Rev Microbiol* 12, 505–518.
- Li S, Fernandez JJ, Fabritius AS, Agard DA, Winey M (2022). Electron cryotomography structure of axonemal doublet microtubule from. *Life Sci Alliance* 5, e202101225.
- Lukeš J, Spejler D, Ziková A, Alfonso JD, Hashimi H, Field MC (2023). Trypanosomes as a magnifying glass for cell and molecular biology. *Trends Parasitol* 39, 902–912.
- Ma M, Stoyanova M, Rademacher G, Dutcher SK, Brown A, Zhang R (2019). Structure of the decorated ciliary doublet microtubule. *Cell* 179: 909–922.e12.
- Mendes Maia T, Gogendeau D, Penner C, Janke C, Basto R (2014). Bug22 influences cilium morphology and the post-translational modification of ciliary microtubules. *Biol Open* 3: 138–151.
- Nicasro D, Fu X, Heuser T, Tso A, Porter ME, Linck RW (2011). Cryo-electron tomography reveals conserved features of doublet microtubules in flagella. *Proc Natl Acad Sci USA* 108, E845–E853.
- Oberholzer M, Langousis G, Nguyen HT, Saada EA, Shimogawa MM, Jonsson ZO, Nguyen SM, Wohlschlegel JA, Hill KL (2011). Independent analysis of the flagellum surface and matrix proteomes provides insight into flagellum signaling in mammalian-infectious Trypanosoma brucei. *Mol Cell Proteomics* 10, M111.010538.
- Oberholzer M, Lopez MA, Ralston KS, Hill KL (2009). Approaches for functional analysis of flagellar proteins in African trypanosomes. *Methods Cell Biol* 93, 21–57.
- Owa M, Uchihashi T, Yanagisawa HA, Yamano T, Iguchi H, Fukuzawa H, Wakabayashi KI, Ando T, Kikkawa M (2019). Inner lumen proteins stabilize doublet microtubules in cilia and flagella. *Nat Commun* 10, 1143.
- Papagni R, Novara R, Minardi ML, Frallonardo L, Panico GG, Pallara E, Cotugno S, Ascoli Bartoli T, Guido G, De Vita E, et al. (2023). Human African Trypanosomiasis (sleeping sickness): Current knowledge and future challenges. *Front Trop Dis* 4.
- Ralston KS, Hill KL (2006). Trypanin, a component of the flagellar dynein regulatory complex, is essential in bloodstream form African trypanosomes. *PLoS Pathog* 2, 873–882.e101.
- Ralston KS, Hill KL (2008). The flagellum of Trypanosoma brucei: new tricks from an old dog. *Int J Parasitol* 38, 869–884.
- Ralston KS, Lerner AG, Diener DR, Hill KL (2006). Flagellar motility contributes to cytokinesis in Trypanosoma brucei and is modulated by an evolutionarily conserved dynein regulatory system. *Eukaryot Cell* 5, 696–711.
- Rao SPS, Barrett MP, Dranoff G, Faraday CJ, Gimpelewicz CR, Hailu A, Jones CL, Kelly JM, Lazdins-Helds JK, Mäser P, et al. (2019). Drug discovery for kinetoplastid diseases: Future directions. *ACS Infect Dis* 5, 152–157.
- Redmond S, Vadivelu J, Field MC (2003). RNAi: An automated web-based tool for the selection of RNAi targets in Trypanosoma brucei. *Mol Biochem Parasitol* 128, 115–118.
- Robinson DR, Sherwin T, Ploubidou A, Byard EH, Gull K (1995). Microtubule polarity and dynamics in the control of organelle positioning, segregation, and cytokinesis in the trypanosome cell cycle. *J Cell Biol* 128, 1163–1172.
- Rotureau B, Ooi CP, Huet D, Perrot S, Bastin P (2014). Forward motility is essential for trypanosome infection in the tsetse fly. *Cell Microbiol* 16, 425–433.
- Saada EA, Kabutu ZP, Lopez M, Shimogawa MM, Langousis G, Oberholzer M, Riestra A, Jonsson ZO, Wohlschlegel JA, Hill KL (2014). Insect stage-specific receptor adenylate cyclases are localized to distinct subdomains of the Trypanosoma brucei flagellar membrane. *Eukaryot Cell* 13, 1064–1076.
- Sáez Conde J, Dean S (2022). Structure, function and druggability of the African trypanosome flagellum. *J Cell Physiol* 237, 2654–2667.
- Salmon D, Vanwalleghem G, Morias Y, Deneud J, Krumbholz C, Lhomme F, Bachmaier S, Kador M, Gossmann J, Dias FB, et al. (2012). Adenylate cyclases of Trypanosoma brucei inhibit the innate immune response of the host. *Science* 337, 463–466.
- Serricchio M, Bütkofer P (2011). Trypanosoma brucei: a model microorganism to study eukaryotic phospholipid biosynthesis. *FEBS J* 278, 1035–1046.
- Shaw S, DeMarco SF, Rehmann R, Wenzler T, Florini F, Roditi I, Hill KL (2019). Flagellar cAMP signaling controls trypanosome progression through host tissues. *Nat Commun* 10, 803.
- Sherwin T, Gull K (1989). The cell division cycle of Trypanosoma brucei brucei: timing of event markers and cytoskeletal modulations. *Philos Trans R Soc Lond Ser B Biol Sci* 323, 573–588.
- Shimogawa MM, Ray SS, Kivalu N, Zhang Y, Geng Q, Ozcan A, Hill KL (2018). Parasite motility is critical for virulence of African trypanosomes. *Sci Rep* 8, 9122.
- Shimogawa MM, Wijono AS, Wang H, Zhang J, Sha J, Szombathy N, Vadakkan S, Pelayo P, Jonnalagadda K, Wohlschlegel J, et al. (2023). FAP106 is an interaction hub for assembling microtubule inner proteins at the cilium inner junction. *Nat Commun* 14, 5225.
- Stoddard D, Zhao Y, Bayless BA, Gui L, Louka P, Dave D, Suryawanshi S, Tomasi RF, Dupuis-Williams P, Baroud CN, et al. (2018). Tetrahymena RIB72A and RIB72B are microtubule inner proteins in the ciliary doublet microtubules. *Mol Biol Cell* 29, 2566–2577.
- Sunter JD, Varga V, Dean S, Gull K (2015). A dynamic coordination of flagellum and cytoplasmic cytoskeleton assembly specifies cell morphogenesis in trypanosomes. *J Cell Sci* 128, 1580–1594.
- Valverde Mordt O, Tarral A, Strub-Wourgaft N (2022). Development and introduction of fexinidazole into the global human African trypanosomiasis program. *Am J Trop Med Hyg* 106, 61–66.
- Velez-Ramirez DE, Shimogawa MM, Ray SS, Lopez A, Rayatpisheh S, Langousis G, Gallagher-Jones M, Dean S, Wohlschlegel JA, Hill KL (2021). APEX2 proximity proteomics resolves flagellum subdomains and identifies flagellum tip-specific proteins in Trypanosoma brucei. *mSphere* 6, e01090–20.
- Vincensini L, Blisnick T, Bastin P (2011). 1001 model organisms to study cilia and flagella. *Biol Cell* 103, 109–130.
- Wickstead B, Ersfeld K, Gull K (2002). Targeting of a tetracycline-inducible expression system to the transcriptionally silent minichromosomes of Trypanosoma brucei. *Mol Biochem Parasitol* 125, 211–216.
- Wirtz E, Leal S, Ochatt C, Cross GA (1999). A tightly regulated inducible expression system for conditional gene knock-outs and dominant-

- negative genetics in *Trypanosoma brucei*. *Mol Biochem Parasitol* 99, 89–101.
- Yanagisawa HA, Mathis G, Oda T, Hirono M, Richey EA, Ishikawa H, Marshall WF, Kikkawa M, Qin H (2014). FAP20 is an inner junction protein of doublet microtubules essential for both the planar asymmetrical waveform and stability of flagella in *Chlamydomonas*. *Mol Biol Cell* 25, 1472–1483.
- Zhang J, Wang H, Imhof S, Zhou X, Liao S, Atanasov I, Hui WH, Hill KL, Zhou ZH (2021). Structure of the trypanosome paraflagellar rod and insights into non-planar motility of eukaryotic cells. *Cell Discov* 7, 51.
- Zhou Q, Liu B, Sun Y, He CY (2011). A coiled-coil- and C2-domain-containing protein is required for FAZ assembly and cell morphology in *Trypanosoma brucei*. *J Cell Sci* 124, 3848–3858.